

mTOR/Raptor signaling is critical for skeletogenesis in mice through the regulation of Runx2 expression

Qinggong Dai^{1,2}, Zhan Xu², Xuhui Ma³, Ningning Niu², Siru Zhou⁴, Furong Xie¹, Lingyong Jiang⁴, Jun Wang^{*1} and Weiguo Zou^{*2}

The mammalian target of rapamycin (mTOR)/regulatory-associated protein of mTOR (Raptor) pathway transmits and integrates different signals including growth factors, nutrients, and energy metabolism. Nearly all these signals have been found to play roles in skeletal biology. However, the contribution of mTOR/Raptor to osteoblast biology *in vivo* remains to be elucidated as the conclusions of recent studies are controversial. Here we report that mice with a deficiency of either *mTOR* or *Raptor* in preosteoblasts exhibited clavicular hypoplasia and delayed fontanelle fusion, similar to those found in human patients with cleidocranial dysplasia (CCD) haploinsufficient for the transcription factor *runt-related transcription factor 2* (*Runx2*) or those identified in *Runx2*^{+/-} mice. Mechanistic analysis revealed that the mTOR-Raptor-S6K1 axis regulates *Runx2* expression through phosphorylation of estrogen receptor α , which binds to Distal-less homeobox 5 (DLX5) and augments the activity of *Runx2* enhancer. Moreover, heterozygous mutation of raptor in osteoblasts aggravates the bone defects observed in *Runx2*^{+/-} mice, indicating a genetic interaction between *Raptor* and *Runx2*. Collectively, these findings reveal that mTOR/Raptor signaling is essential for bone formation *in vivo* through the regulation of *Runx2* expression. These results also suggest that a selective mTOR/Raptor antagonist, which has been developed for treatment of many diseases, may have the side effect of causing bone loss.

Cell Death and Differentiation (2017) 24, 1886–1899; doi:10.1038/cdd.2017.110; published online 7 July 2017

Osteoblasts, the bone-forming cells active during bone development and remodeling,^{1,2} are derived from bone marrow mesenchymal stem cells (BMSCs). The differentiation of osteoblasts from BMSCs is controlled by transcription factors that are expressed in a defined temporal and spatial sequence. Among them, *runt-related transcription factor 2* (*Runx2*) is considered to be the master transcription factor^{3,4} as mice deficient in *Runx2* exhibit a lack of mineralization in the skeleton and absence of mature osteoblasts.⁵ *Runx2*-heterozygous mice display clavicular hypoplasia and delayed closure of the fontanelles, a phenotype resembling the cleidocranial dysplasia (CCD) syndrome caused by mutations of *Runx2* in humans.⁶ *Runx2* expression at appropriate times and sites is essential for bone development and bone remodeling. However, regulation of *Runx2* expression, especially the upstream signaling pathways involved, has not been completely clarified.

The mammalian/mechanistic target of rapamycin (mTOR) is an evolutionarily conserved protein kinase. mTOR functions in two structurally and functionally distinct multiprotein complexes, namely mTORC1 and mTORC2,⁷ which are distinct in their unique components and downstream targets. mTORC1 contains Raptor and is sensitive to rapamycin, while mTORC2 contains Rictor and is resistant to rapamycin. S6 kinase1

(S6K1) is the mTORC1 downstream target and can phosphorylate a series of substrates including estrogen receptor α (ER α) and S6 ribosomal protein (S6) to control gene transcription, protein synthesis, and other biological processes.^{8–10} mTORC1 signaling is considered as the check-point of several extracellular and intracellular signals including growth factors, nutrients, energy metabolism and stress¹¹ and has been the target for drug development in many diseases,¹¹ which highlights the necessity of studying the role of mTORC1 in osteoblasts and bone development to monitor and avoid possible side effects on bone.

Recently, different studies of the role of mTORC1 signaling in osteoblast differentiation and bone development produced controversial results.¹² Previous *in vitro* studies shown that mTORC1 can activate^{13,14} or inhibit¹⁵ osteogenesis, and these controversies may be resulted from the differences in the cell types or cell differentiation-stages examined. Furthermore, disturbing of mTOR signaling in osteoblast-lineage cells induced various skeletal disorders. A mouse model with increased mTORC1 activity in neural crest-derived cells due to deletion of *tuberous sclerosis 1* (*Tsc1*) led to increased bone mass through enlargement of the osteoprogenitor pool.¹⁶ Interestingly, two independent studies indicated that osteoblast-specific inactivation of *Tsc* complex caused osteoblasts to

¹Department of Pediatric Dentistry, Shanghai Ninth People's Hospital, School of Medicine, Shanghai Jiaotong University; Shanghai Key Laboratory of Stomatology, Shanghai 200011, China; ²State Key Laboratory of Cell Biology, CAS Center for Excellence in Molecular Cell Science, Shanghai Institute of Biochemistry and Cell Biology, Chinese Academy of Sciences; University of Chinese Academy of Sciences, Shanghai 200031, China; ³Department of Oral and Maxillofacial-Head and Neck Oncology, Ninth People's Hospital, Shanghai Jiaotong University School of Medicine, Shanghai Key Laboratory of Stomatology, Shanghai 200011, China and ⁴Center of Craniofacial Orthodontics, Department of Oral and Cranio-Maxillofacial Science, Ninth People's Hospital, Shanghai Jiaotong University School of Medicine, Shanghai Key Laboratory of Stomatology, Shanghai 200011, China

*Corresponding author: J Wang, Department of Pediatric Dentistry, Shanghai Ninth People's Hospital, School of Medicine, Shanghai Jiaotong University, No. 639, Zhi Zao Ju Road, Shanghai 200011, China. Tel: +86 21 23271699; Fax: +86 21 23271699; E-mail: wangjun202@126.com or W Zou, Shanghai Institute of Biochemistry and Cell Biology, Chinese Academy of Sciences; University of Chinese Academy of Sciences, 320 Yueyang Road, SIBCB Building, Rm 1401, Shanghai 200031, China. Tel: +86 21 54921320; Fax: +86 21 54921320; E-mail: zouwg94@sibcb.ac.cn

Received 07.2.17; revised 08.5.17; accepted 31.5.17; Edited by M Piacentini; published online 07.7.17

differentiate poorly and produce disorganized bone.^{17,18} On the other hand, Chen *et al.* reported that enhanced mTORC1 signaling due to heterozygous mutations in the *fibrillin-1* gene resulted in osteopenia.¹⁹ Furthermore, decreased mTORC1 signaling with deletion of *mTOR* or *Raptor* in mesenchyme resulted in death shortly after birth and skeletal discrepancy.²⁰ *Raptor* deletion in Osterix-expressing preosteoblasts led to osteopenia.²¹ In contrast, an *in vitro* study showed that depletion of *Raptor* promoted osteoblast differentiation of BMSCs.²² Taken together, these data reveal that the role of mTORC1 signaling in osteoblasts is still ambiguous and the underlying mechanisms have not been fully illuminated.

In the present study, we found that loss of mTORC1 signaling in preosteoblasts through the deletion of *mTOR* or *Raptor* in mice induced severe skeletal defects secondary to impaired osteogenesis and osteoblast differentiation. Further molecular mechanism studies revealed that the mTOR-Raptor-S6K1 axis could promote osteoblast differentiation through regulating *Runx2* expression by augmenting the activity of *Runx2* enhancer.

Results

mTOR deficiency in preosteoblasts causes a CCD phenotype with impaired osteoblast differentiation. To determine the role of mTOR signaling in preosteoblasts *in vivo*, we generated conditional *mTOR* knockout mice (*mTOR^{fl/fl};Osx-cre*, hereafter *mTOR^{Osx}*) (Figure 1a) by crossing *mTOR^{fl/fl}* mice with *Osx-cre* mice, a transgenic line in which Cre activation is confined to osteoblast precursors. Western blot assay confirmed the loss of mTOR protein in parietal bones from *mTOR^{Osx}* newborns (Figure 1b). Compared to WT mice and mice heterozygous for the *mTOR* floxed allele (*mTOR^{fl/+};Osx-cre*, hereafter *mTOR^{Osx/+}*), *mTOR^{Osx}* mice showed slower growth rate (Figures 1c and d). Alizarin red and Alcian blue staining showed although newborn *mTOR^{Osx}* mice had similar skeletal size to their WT littermates (Figure 1e), *mTOR^{Osx}* mice exhibited the CCD phenotype with clavicular hypoplasia and hypomineralization of the calvarium (Figure 1f), features of mice heterozygous for *Runx2*.

In addition to the clavicular and calvarial phenotypes, *mTOR^{Osx}* mice displayed a substantial reduction in bone mass. As shown in Figures 2a and b, femoral trabecular bone of 4-week-old male *mTOR^{Osx}* mice displayed an approximately 70% reduction in bone volume fraction (BV/TV) compared to WT littermates while *mTOR^{Osx/+}* showed an intermediate effect (Figure 2b). The significant reduction in bone mass between *mTOR^{Osx}* and *mTOR^{Osx/+}* confirmed that the decreased bone density in *mTOR^{Osx}* mice is due to the loss of *mTOR* in osteoblasts, not to the presence of the Cre transgene. *mTOR^{Osx}* mice also displayed a decrease of trabecular number (Tb.N., Figure 2c) and trabecular thickness (Tb.Th., Figure 2d). *mTOR^{Osx}* mice also displayed a dramatic reduction of the cortical thickness (Ct.Th., Figure 2e).

We next examined whether the abnormal osteogenesis in *mTOR^{Osx}* mice was a result of inadequate osteoblast differentiation. We cultured calvarial cells from *mTOR^{Osx}* and WT mice and found that *mTOR^{Osx}* calvarial cells showed reduced

osteoblast differentiation, revealed by decreased alkaline phosphatase (ALP) activity and fewer calcified nodules, measured by alizarin red staining (Figure 2f). Consistent with the reduced ossification and osteoblast differentiation, expression of the characteristic osteoblast marker genes, *collagen 1a1* (*Col1a1*, Figures 2i and j) and *osteocalcin* (*Ocn*, Figures 2i and k) were reduced in osteoblasts from *mTOR^{Osx}* mice *in vivo* accompanied with the decrease of *Runx2* expression (Figures 2g and h). Taken together, the CCD phenotype and reduced bone mass, possibly secondary to impaired osteoblastic differentiation in *mTOR^{Osx}* mice, supported the hypothesis that mTOR is critical for bone development.

Raptor deficiency in preosteoblasts also causes a CCD phenotype and reduced bone mass with impaired osteoblast differentiation.

To further investigate the specific contribution of mTORC1 in osteoblasts, we generated conditional *Raptor* knockout mice (*Rap^{fl/fl};Osx-cre*, hereafter *Rap^{Osx}*) by mating *Rap^{fl/fl}* mice with *Osx-cre* mice (Figure 3a). Western blot assay revealed the loss of Raptor protein in parietal bones from *Rap^{Osx}* mice (Figure 3b). Similar to *mTOR^{Osx}* mice, *Rap^{Osx}* mice showed a slower growth pattern after birth (Figures 3c and d). The newborn *Rap^{Osx}* mice also exhibited the CCD phenotype with clavicular hypoplasia and hypomineralization of the calvarium (Figure 3f) although *Rap^{Osx}* mice had similar skeletal size to their WT littermates (Figure 3e). Hypocalcification of calvarial and clival bones were confirmed in 4-week-old *Rap^{Osx}* mice by micro-CT and X-ray analysis (Figure 3g). Moreover, 4-week-old *Rap^{Osx}* mice had an osteopenic phenotype with decreased BV/TV, Tb.N., Tb.Th. and Ct.Th. in the femur (Figures 4a–e). Further, 6-month-old *Rap^{Osx}* mice showed CCD phenotype with clavicular hypoplasia and hypomineralization of the calvarium (Supplementary Figure 1A). Micro-CT scanning confirmed calvarial hypoplasia (Supplementary Figure 1B) and showed decreased BV/TV, Tb.N., Tb.Th. and Ct.Th. in *Rap^{Osx}* mice in comparison with WT mice (Supplementary Figure 1C–G). The significant difference between *Rap^{Osx}* mice and *Rap^{Osx/+}* mice accompanied with the skeletal defects in 6-month-old *Rap^{Osx}* mice confirmed that it is the loss of *Raptor* in osteoblasts, not the presence of the Cre transgene, that is responsible for the bone defects in *Rap^{Osx}* mice.

Primary osteoblast cultures from *Rap^{Osx}* mice exhibited decreased osteoblast differentiation, determined by decreased ALP activity and mineralized matrix production (Figure 4f). Consistent with this, *Rap^{Osx}* mice displayed decreased *Col1a1* and *Ocn* mRNA expression *in vivo* (Figures 4i–k) as well as reduced *Runx2* protein expression (Figures 4g and h). The similar bone phenotype between *Rap^{Osx}* mice and *mTOR^{Osx}* mice supported the hypothesis that mTOR drives skeletal development mainly via the mTORC1 complex. The decreased bone mass in both *mTOR^{Osx}* and *Rap^{Osx}* mice might arise through increased bone resorption. To address this, we analyzed femurs from 4-week-old mice for the presence of tartrate-resistant acid phosphatase (TRAP)-positive osteoclasts. In comparison with WT littermates, both *mTOR^{Osx}* and *Rap^{Osx}* mice displayed a modest decrease in TRAP-positive osteoclasts (Supplementary Figures 2A and B), indicating that the bone lesions in *mTOR^{Osx}* or *Rap^{Osx}* mice are attributable to impaired bone formation as opposed to

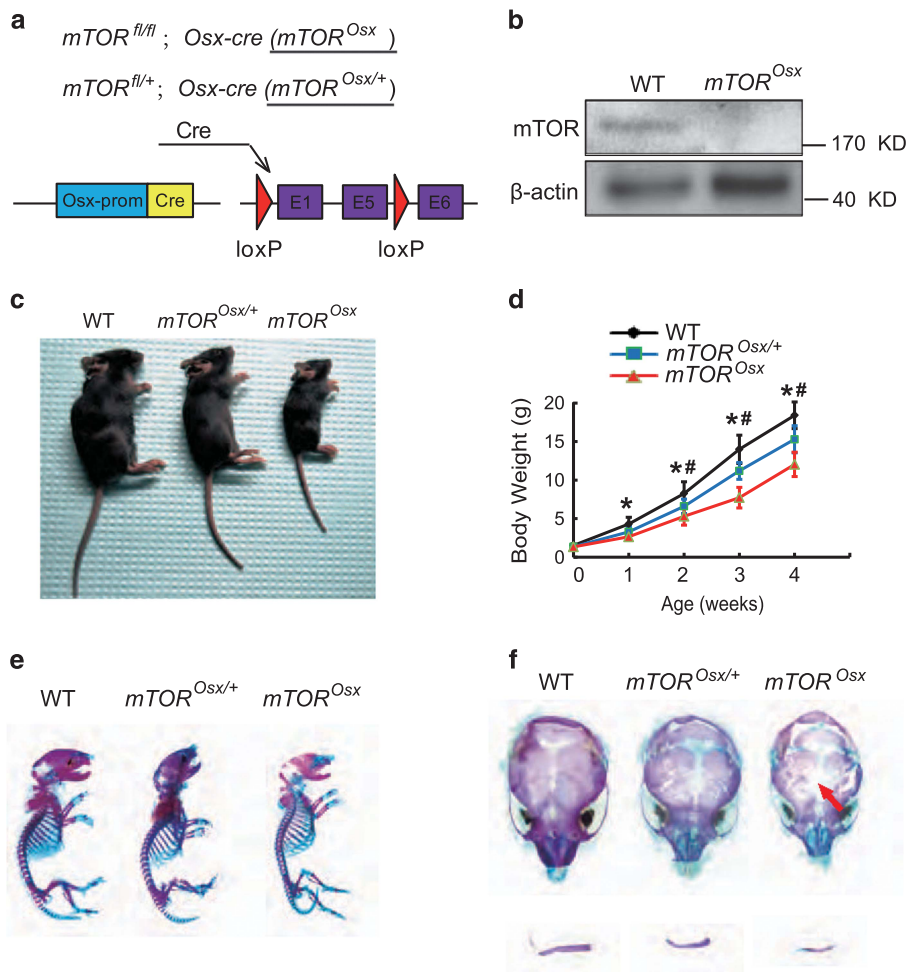


Figure 1 Preosteoblast-specific knockout of *mTOR*-induced CCD-like bone defects in mice. (a) Illustration of *mTOR* deletion in *Osx*-expressing preosteoblasts. (b) Western blot assay of *mTOR* in parietal bone lysate of WT and $mTOR^{Osx}$ newborns. (c) Representative view of 4-week-old WT, $mTOR^{Osx/+}$ and $mTOR^{Osx}$ mice. (d) Body weight of male WT, $mTOR^{Osx/+}$ and $mTOR^{Osx}$ littermates measured at different age points ($n=5$ for each group, *t*-test). Data represent means \pm s.d. * $P < 0.05$ in comparison with WT mice, # $P < 0.05$ when compared with $mTOR^{Osx/+}$ mice. (e) Representative images of skeleton of WT, $mTOR^{Osx/+}$ and $mTOR^{Osx}$ newborn littermates by alcian blue and alizarin red staining. (f) Clavicular hypoplasia and calvarial hypomineralization of $mTOR^{Osx}$ newborns. Arrow indicates calvarial lesions in $mTOR^{Osx}$ mice

decreased bone resorption. Further confirming the decrease in osteoblast activity, 4-week-old Rap^{Osx} mice demonstrated a decreased bone formation rate (BFR) and mineral apposition rate (MAR) as determined by alizarin red and calcein labeling (Figures 4l and m). Collectively, these data support the hypothesis that mTOR/Raptor (mTORC1) is critical for osteoblast activity and anabolic bone formation.

S6K1 is a downstream factor of mTOR/Raptor in osteoblasts. S6K1 is the most important downstream regulator of mTORC1 and plays crucial roles in development and aging. To determine whether S6K1 could function downstream of mTOR/Raptor in osteoblasts, we analyzed the level of phospho-S6K1 in 7-day-old mice by immunohistochemistry. An antibody specific to phospho-S6K1 (T389) demonstrated robust signal in osteoblast-lining cells in subchondral trabecular bone and in adjacent osteocytes (Figures 5a and d). At the same time, both $mTOR^{Osx}$ and Rap^{Osx} mice showed decreased S6K1 phosphorylation in comparison with their WT littermates (Figures 5a,b,d and e).

We also analyzed lysates from parietal bone of $mTOR^{Osx}$ and Rap^{Osx} newborn mice. As shown in Figures 5c and f, although the expression of S6K1 is comparable between WT mice and $mTOR^{Osx}$ or Rap^{Osx} mice, the level of phosphorylation of S6K1 in $mTOR^{Osx}$ or Rap^{Osx} mice was dramatically decreased. To examine whether the reduction of S6K1 phosphorylation could be responsible for impaired osteoblast differentiation, the expression of constitutively-active S6K1 (CAS6K1, T390E) was enforced in *Raptor*-deficient osteoblasts. CAS6K1 overexpression was determined by immunoblotting (Figure 5h) and the efficiency of CAS6K1 was confirmed by increased phosphorylation of ribosomal protein S6 (P-S6, S 235/236). Furthermore, the impaired osteoblast differentiation of Rap^{Osx} calvarial cells was significantly improved by CAS6K1 overexpression as demonstrated by increased ALP activity and mineralized nodule formation (Figure 5g). Similarly, enforced expression of CAS6K1 rescued the decreased expression of *Runx2* (Figure 5i), *Col1a1* (Figure 5j) and *Ocn* (Figure 5k) in *Raptor*-deficient calvarial cells. These data demonstrate that the

impaired S6K1 activity is responsible for the impaired osteoblast differentiation of *Raptor*-deficient calvarial osteoblasts.

The mTOR-Raptor-S6K1 axis signaling regulates *Runx2* expression in osteoblasts. Both *mTOR^{Osx}* and *Rap^{Osx}* mice displayed a striking similarity to *Runx2^{+/-}* mice with

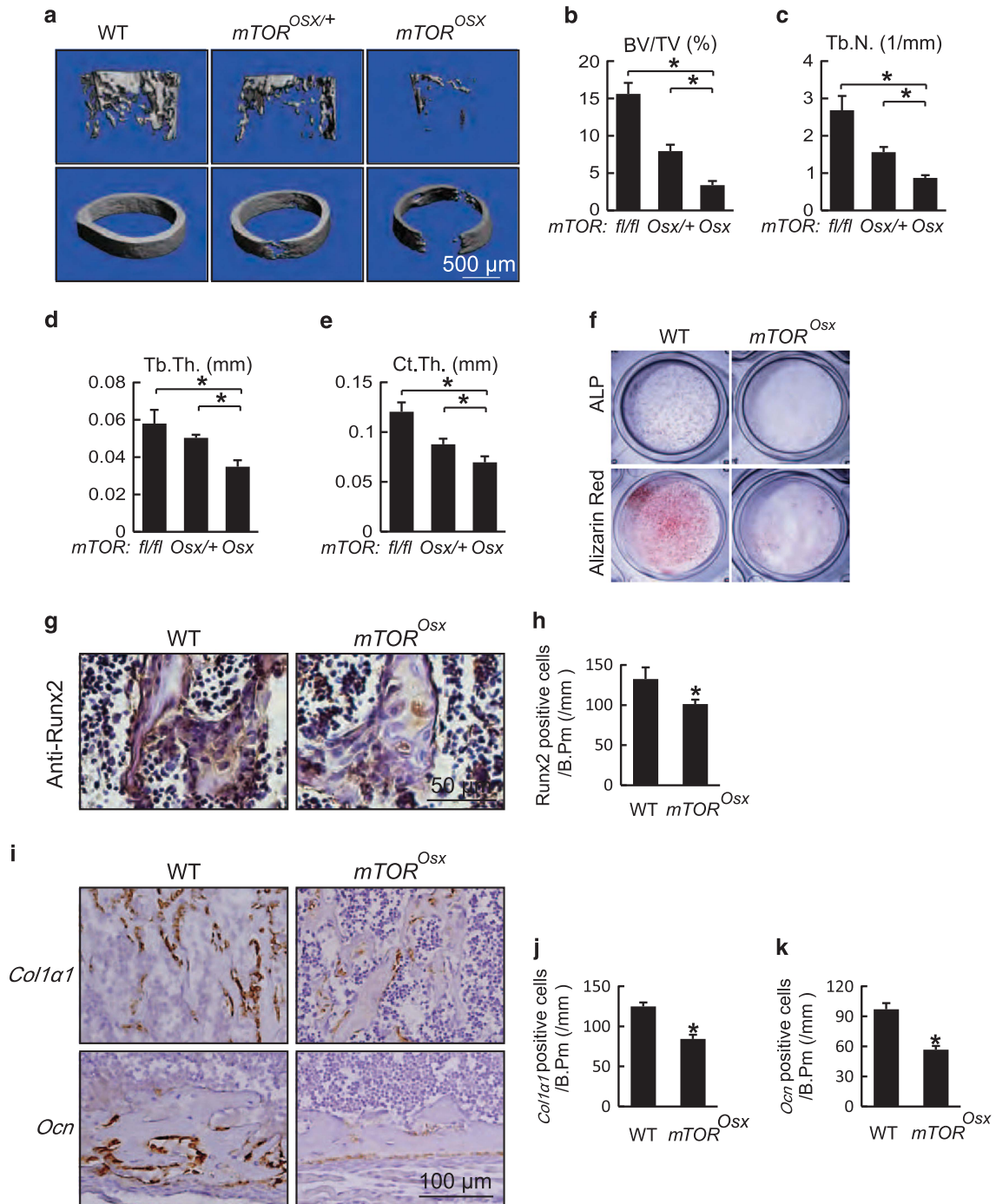


Figure 2 *mTOR* deficiency in osteoblasts resulted in reduced bone mass with impaired osteoblast differentiation. (a) Micro-CT images of femur from 4-week-old WT, *mTOR^{Osx/+}* and *mTOR^{Osx}* littermates. (b–e) Quantitative parameters of Micro-CT. BV/TV: bone volume/total volume, Tb.N.: trabecular number, Tb.Th.: trabecular thickness, Ct.Th.: cortical thickness. Data represent means \pm s.d. * $P < 0.05$, $n = 5$. (f) Calvarial osteoblasts were cultured with osteogenic medium from 5-day-old WT and *mTOR^{Osx}* littermates. ALP staining and alizarin red staining were performed to analyze osteoblast differentiation on the 7th and 14th day respectively. (g) Immunohistochemistry for Runx2 of distal femur from 7-day-old WT and *mTOR^{Osx}* mice. (h) Number of Runx2-positive osteoblasts counted in the distal femur from 7-day-old WT and *mTOR^{Osx}* mice. Data represent means \pm s.d. * $P < 0.05$, $n = 3$. (i) *In situ* hybridization for *Col1a1* and *Ocn* in femur from 7-day-old WT and *mTOR^{Osx}* littermates. (j) Number of *Col1a1*-positive osteoblasts counted in the trabecular bone of distal femur from 7-day-old WT and *mTOR^{Osx}* littermates. Data represent means \pm s.d. * $P < 0.05$, $n = 3$. (k) Number of *Ocn*-positive osteoblasts calculated in the cortical bone of distal femur from 7-day-old WT and *mTOR^{Osx}* littermates. Data represent means \pm s.d. * $P < 0.05$, $n = 3$

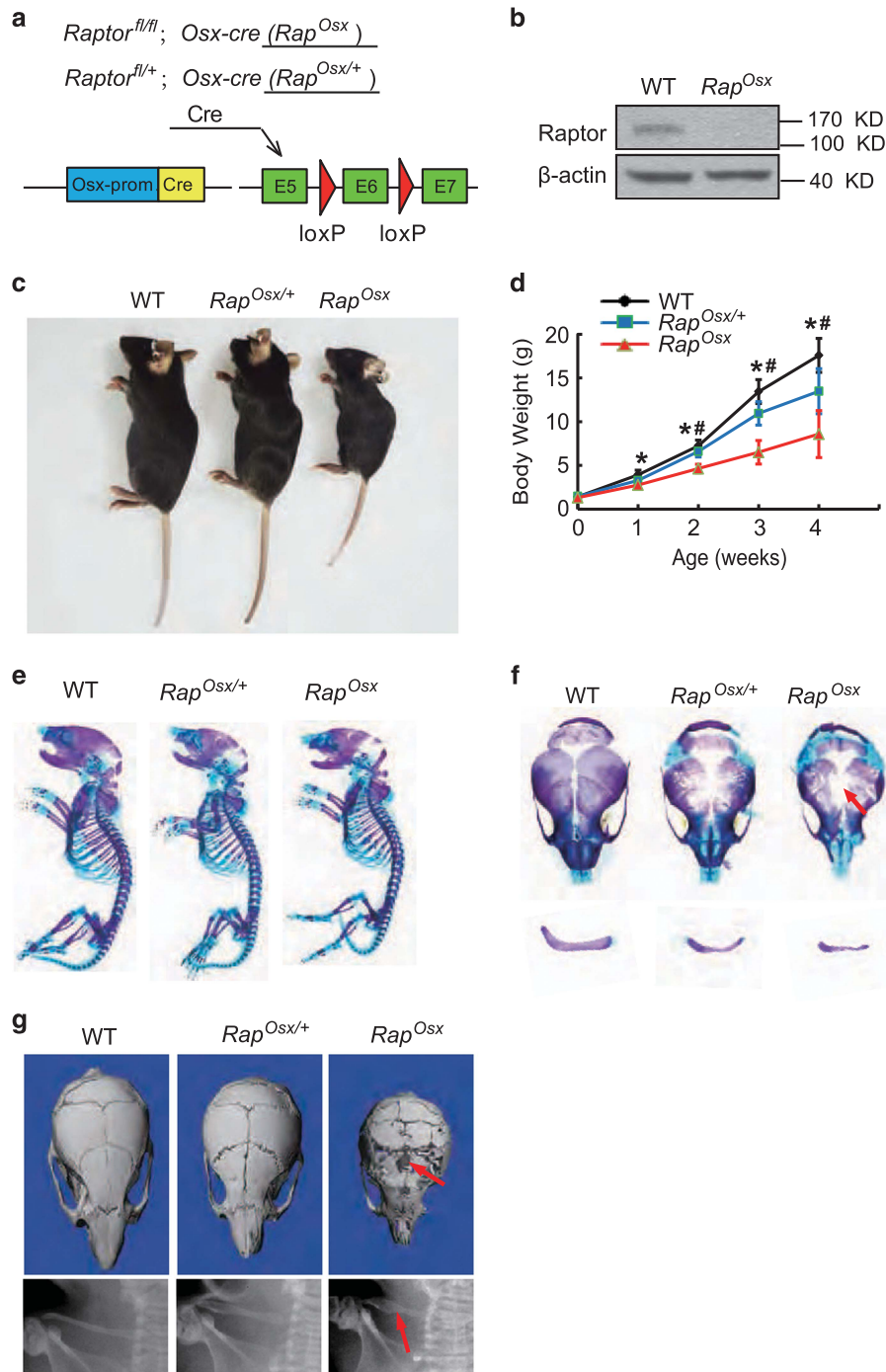


Figure 3 Ablation of *Raptor* in preosteoblasts resulted in CCD-like phenotype. (a) Illustration of *Raptor* deletion in *Osx*-expressing preosteoblasts. (b) Expression of *Raptor* in parietal bone from WT and Rap^{Osx} newborns. (c) Representative view of 4-week-old WT, $Rap^{Osx/+}$ and Rap^{Osx} mice. (d) Body weight of male WT, $Rap^{Osx/+}$ and Rap^{Osx} littermates measured at different age points ($n=5$ for each group, *t*-test). Data represent means \pm s.d. * $P < 0.05$ in comparison with WT mice, # $P < 0.05$ when compared with $Rap^{Osx/+}$ mice. (e) Representative images of skeleton from WT, $Rap^{Osx/+}$ and Rap^{Osx} newborn littermates by alcian blue and alizarin red staining. (f) Clavicular hypoplasia and calvarium hypomineralization of Rap^{Osx} newborns. Arrow indicates calvarial lesions in $mTOR^{Osx}$ mice. (g) Micro-CT of skulls and X-ray of clavicles from 4-week-old WT, $Rap^{Osx/+}$ and Rap^{Osx} mice. Arrow indicates calvarial lesions and hypoplastic clavicle in $mTOR^{Osx}$ mice

features including CCD phenotype and reduced bone mass, suggesting that mTORC1 may regulate *Runx2* expression. This hypothesis was supported by the facts that both $mTOR^{Osx}$ and Rap^{Osx} mice displayed decreased *Runx2*

protein expression *in vivo* (Figures 2g and h and Figures 4g and h) and that enforced expression of CAS6K1 increased *Runx2* mRNA level (Figure 5i). Likewise, CAS6K1 was able to rescue the decreased *Runx2* expression in

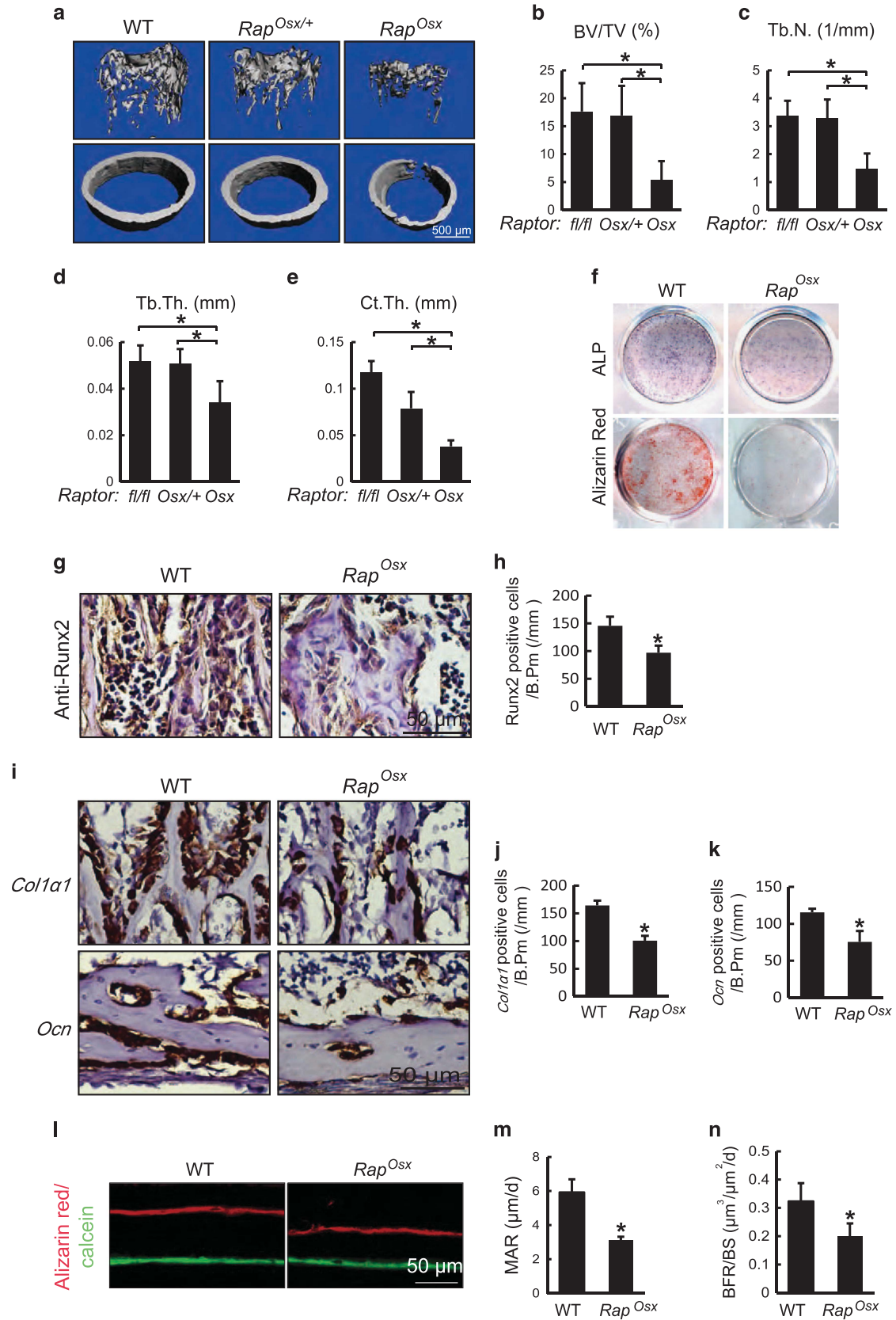
Raptor-deficient osteoblasts at the protein level (Figure 5h). To exclude the possibility that the decreased *Runx2* expression is due to the different cell populations, we cultured BMSCs from *Raptor*^{fl/fl} mice and then infected the cells with adenovirus expressing GFP and CRE recombinase. As shown in Figure 6a, CRE adenovirus led to reduced expression of Raptor accompanied by decreased levels of Runx2 protein. Thus, the effect of *Raptor* on regulating *Runx2* expression cannot be attributed to differences in cell population. Consistent with the lower Runx2 protein level, CRE adenovirus caused impaired osteoblast differentiation (Figure 6b). The change of Runx2 protein level was reflected in a dramatic decrease of Runx2 mRNA level by CRE adenovirus (Figure 6c), which was accompanied by a decrease of *Runx2* downstream osteogenic genes such as *Col1a1* (Figure 5d) and *Ocn* (Figure 5e). These data suggest that mTORC1 could regulate *Runx2* expression at the transcript level. To further determine whether the impaired osteoblast differentiation induced by inactivation of mTORC1 was due to the reduction of *Runx2* expression, we analyzed the effects of enforced Runx2 expression on *Raptor*-deficient osteoblasts. Calvarial osteoblastic cells from *Rap*^{Osx} mice were infected with lentivirus expressing Runx2 (Lenti-Runx2) or GFP (Lenti-GFP). Western blot assay confirmed Runx2 overexpression in *Rap*^{Osx} osteoblasts (Figure 6f). The decreased osteoblast differentiation in *Rap*^{Osx} calvarial cells was rescued by *Runx2* overexpression as determined by ALP activity and mineralized nodule formation (Figure 6g). Consistent with this, the decreased expression of *Runx2* downstream genes including *Col1a1* and *Ocn* was rescued by *Runx2* overexpression (Figures 6h and i). These results indicated that mTOR/Raptor-S6K1 signaling promoted skeletal development and osteoblast differentiation through regulation of *Runx2* expression.

S6K1 regulates *Runx2* expression via its enhancer. Next, we intended to investigate the mechanisms by which mTORC1 regulates *Runx2* expression. First, we examined the effects of CAS6K1 on activity of the *Runx2* promoter by an *in vitro* luciferase assay. As shown in Supplementary Figure 3A, CAS6K1 had no effects on activation of the *Runx2* promoter. Kawane *et al.* demonstrated that the enhancer of *Runx2* plays an important role in directing *Runx2* expression in osteoblasts.²³ Consequently, we next examined the effects of CAS6K1 on the *Runx2* enhancer. As shown in Figure 7a, the activity of the luciferase reporter driven by the 3x 89 bp *Runx2* core enhancer (*Runx2* enhancer) was promoted by CAS6K1 expression. Furthermore, we found *Runx2* enhancer activity decreased in *Rap*^{Osx} calvarial cells compared with WT group (Figure 7b), which confirmed mTORC1-S6K1 may regulate *Runx2* expression through its enhancer. The *Runx2* core enhancer is bound by Distal-less homeobox 5 (DLX5) and MEF2C,²³ so we examined the effects of CAS6K1 on DLX5- and MEF2C-induced *Runx2* enhancer activity. As shown in Figure 7c, CAS6K1 could increase DLX5-induced *Runx2* enhancer activity, but not MEF2C (Supplementary Figure 3B). However, we were unable to detect any interaction between S6K1 and DLX5 by co-immunoprecipitation (coIP) experiments (Supplementary Figure 1C). This is consistent with the fact that DLX5 does not contain the S6K1

phosphorylation motif RxRxxS/T (where x could be any amino acid). Thus, S6K1 may regulate *Runx2* enhancer activity by phosphorylating proteins other than DLX5. It has been reported that S6K1 promotes estrogen receptor α (ER α) activity by phosphorylating it on S167 in cancer cells^{9,24} and ER α can regulate *Runx2* expression in osteoblast progenitors.^{25–27} We hypothesized that S6K1 may regulate *Runx2* enhancer activity by phosphorylating ER α . First, we confirmed the protein interaction between S6K1 and ER α (Figure 7d). Next, we found that ER α could increase the activity of *Runx2* enhancer, while co-transfection of CAS6K1 was able to promote this effect (Figure 7e). We then examined whether mutation of the S6K1 phosphorylation motif renders ER α refractory to activation by S6K1. The S6K1 phosphorylation site of ER α was mutated by converting Ser¹⁷¹ into alanine.²⁸ We found that when compared with WT ER α , ER α -S171A was resistant to CAS6K1 effects on the activity of *Runx2* enhancer (Figure 7f). These data indicate that S6K1 regulates *Runx2* enhancer activity by phosphorylation of ER α . To further test this hypothesis, we analyzed the phosphorylation of ER α (P-ER α , S167) in 7-day-old *mTOR*^{Osx} and *Rap*^{Osx} mice by immunohistochemistry. As shown in Supplementary Figures 3D,E and Figures 7g and h, P-ER α -positive cells decreased in both *mTOR*^{Osx} and *Rap*^{Osx} mice compared to WT mice, which confirmed that S6K1 regulates *Runx2* enhancer activity by phosphorylation of ER α .

Interestingly, we found that DLX5 and ER α could synergistically increase the activity of *Runx2* enhancer and that CAS6K1 could further promote these effects (Figure 7i). As the 89 bp *Runx2* core enhancer lacks an ER α binding motif, we hypothesized that ER α might augment *Runx2* enhancer activity through interaction with DLX5. Indeed ER α and DLX5 could interact when both were ectopically expressed in 293T cells (Figure 7j). Next, we confirmed this protein interaction between ER α and DLX5 in calvarial osteoblasts (Figure 7k). To further analyze whether the interaction of ER α and DLX5 was dependent on phosphorylation of ER α , WT and phosphorylation site mutant ER α (ER α -WT, ER α -S171E, ER α -S171A) were co-transfected with DLX5 in 293T cells. As shown in Figure 7l, DLX5 could interact with all three ER α protein, which suggested that the interaction of ER α and DLX5 was independent of ER α phosphorylation and excluded the possibility that mTORC1 regulate *Runx2* enhancer activity by affecting the interaction of ER α and DLX5. Next we analyze the binding of ER α and Dlx5 to *Runx2* enhancer by CHIP-qPCR in *Rap*^{Osx} calvarial osteoblasts. As shown in Figures 7m and n, the binding of ER α and Dlx5 to *Runx2* enhancer decreased in *Rap*^{Osx} calvarial osteoblasts in comparison to the WT groups, which indicated that mTORC1-S6K1 signaling can promote the binding of the transcriptional factors ER α and Dlx5 to *Runx2* enhancer. These data support the hypothesis that the mTOR-Raptor-S6K1 axis can regulate *Runx2* expression via its enhancer, probably by phosphorylating ER α which interacts with DLX5 and augments *Runx2* enhancer activity.

mTORC1 interacts genetically with *Runx2* *in vivo*. Based on the *in vitro* results above, we next questioned whether mTORC1 is an upstream regulator of *Runx2* *in vivo*. We postulated that if mTORC1 indeed regulates expression of



Runx2, then reduced activity of mTORC1 in parallel with *Runx2* haploinsufficiency *in vivo* should aggravate the bone defects in *Runx2*^{+/-} mice. To test this hypothesis, we generated *Rap*^{Osx/+}*Runx2*^{+/-} mutant mice by crossing *Rap*^{Osx/+} and *Runx2*^{+/-} mice and analyzed skeletal preparations from newborn WT, *Rap*^{Osx/+}, *Runx2*^{+/-} and *Rap*^{Osx/+}*Runx2*^{+/-} mice. As shown in Figure 8a, the body weights of *Runx2*^{+/-} and *Rap*^{Osx/+}*Runx2*^{+/-} mice were slightly lower than those of WT and *Rap*^{Osx/+} mice and the skeletons of *Runx2*^{+/-} and *Rap*^{Osx/+}*Runx2*^{+/-} mice were consistently smaller (Figure 8b). *Runx2*^{+/-} mice displayed the previously reported CCD-like phenotype. Heterozygous deletion of Raptor resulted in minor skeletal defects in both the clavicle and calvarium (Figures 8c–e). However, *Rap*^{Osx/+}*Runx2*^{+/-} mice showed far more severe bone defects than *Runx2*^{+/-} mice, including a larger hypoplastic area of the cranial bones (Figures 8c and d) and barely visible clavicles (Figures 8c and e). Taken together, these results suggest a genetic relationship between mTORC1 and *Runx2*, and provide *in vivo* evidence that mTORC1 can regulate osteoblast function through *Runx2*.

Discussion

In the present study, we revealed the critical role of mTOR/Raptor signaling in osteoblasts and bone development through conditional knockout of *mTOR* and *Raptor*, respectively. Deletion of *mTOR* in preosteoblasts induced marked skeletal defects, including dwarfism with short limbs, impaired ossification of the cranial bones, hypoplasia of the clavicles and reduced bone mass, which support the conclusion that mTOR is essential for both endochondral and intramembranous ossification. Further, preosteoblast-specific loss of *Raptor* reproduced almost all skeletal phenotypes of *mTOR*^{Osx} mice, suggesting that mTOR functions mainly through mTORC1 in osteoblasts and osteogenesis. On the other hand, other researchers have found that continuous mTORC1 activation led to bone defects.^{18,19} These results suggested that mTOR signaling is regulated precisely during bone development, and either upregulation or downregulation of mTORC1 signaling may result in bone diseases. Although the precise balance point of mTORC1 signaling in osteoblasts will need to be investigated in further studies, the possible side effects on bone of changes in mTORC1 signaling caused by any agent which has been or is intended to be used as a treatment target in a range of diseases¹¹ should be taken into account.

MSCs can differentiate into multiple lineages including the osteoblast, chondrocyte and adipocyte lineages. While it has been demonstrated that mTOR signaling is essential for both

chondrocyte^{20,29} and adipocyte³⁰ differentiation, there is limited and controversial information available regarding the independent role of mTOR in osteoblast and osteogenesis.¹² In this study, we revealed several lines of evidence showing that inactivation of mTORC1 inhibited osteoblast differentiation and bone formation. First, osteoblast-specific deletion of either *mTOR* or *Raptor* led to decreased expression of osteoblastic markers *in vivo*. Second, BFR was reduced in *Rap*^{Osx} mice. Third, osteoblast differentiation of *Rap*^{Osx} parietal cells was impaired. Taken together, we believe that physiological mTORC1 signaling is essential for osteoblast differentiation and bone formation.

There is limited information available about the mechanisms by which mTORC1 promotes osteoblast differentiation. It has been demonstrated that S6K1 can positively regulate the differentiation of both chondrocytes²⁹ and adipocytes.¹⁰ In our current study, we provided evidence indicating that S6K1 is the major downstream regulator of mTORC1 in osteoblasts and that the mTOR/Raptor-S6K1 axis could promote osteoblast differentiation and osteogenesis.

Mutations of *Runx2* result in CCD in humans and *Runx2*^{+/-} mice exhibited CCD-like phenotypes except for supernumerary teeth.^{4–6} However, some CCD patients do not carry *Runx2* mutations, and a decrease to 70% of wild-type *Runx2* levels can result in CCD syndrome in mice.³¹ These results indicate that CCD may result from other mechanisms that regulate *Runx2* expression. Here, we provided evidence that mTOR/Raptor-S6K1 signaling promotes *Runx2* expression. Preosteoblast-specific deletion of either *mTOR* or *Raptor* results in bone defects, resembling the CCD phenotype and decreased *Runx2* expression *in vivo*. Moreover, *Raptor*-deficient BMSCs and parietal cells displayed reduced *Runx2* expression, and the impaired osteoblast differentiation in *Rap*^{Osx} parietal cells can be rescued by *Runx2* overexpression. The reduced *Runx2* expression in *Rap*^{Osx} parietal cells can be rescued by enforced CAS6K1 expression. Molecular experiments demonstrated that CAS6K1 can augment the activity of *Runx2* enhancer, but not the *Runx2* promoter. Finally, heterozygous *Raptor* in osteoblasts aggravates skeletal phenotypes of *Runx2*^{+/-} mice, supporting a genetic link between mTORC1 signaling and *Runx2*. Taken together, these data suggest that physiological mTORC1 signaling is essential for *Runx2* expression. Meanwhile, hyperactivation of mTORC1 in osteoblasts-induced bone defects were also related to decreased *Runx2* expression.^{18,19}

Our study clarifies the critical role of mTOR/Raptor signaling in osteoblasts and bone development and demonstrates that mTOR-Raptor-S6K1 can regulate *Runx2* expression, providing new sights into skeletal dysplasias such as CCD.

Figure 4 *Raptor* deficiency in osteoblasts displayed reduced bone mass with impaired osteoblast differentiation. (a) Micro-CT images of femur from 4-week-old WT, *Rap*^{Osx/+} and *Rap*^{Osx} littermates. (b–e) Quantitative parameters of Micro-CT. Data represent means ± s.d. **P* < 0.05, *n* = 5. (f) ALP staining and alizarin red staining of WT and *Rap*^{Osx} calvarial cells induced by osteogenic medium. Data represent means ± s.d. **P* < 0.05, *n* = 3. (g) Immunohistochemistry for *Runx2* of distal femur from 7-day-old WT and *Rap*^{Osx} mice. (h) Number of *Runx2*-positive osteoblasts counted in the trabecular bone of distal femur from WT and *Rap*^{Osx} mice. Data represent means ± s.d. **P* < 0.05, *n* = 3. (i) *In situ* hybridization for *Col1α1* and *Ocn* in femur from 7-day-old WT and *Rap*^{Osx} littermates. (j) Number of *Col1α1*-positive osteoblasts counted in the trabecular bone of distal femur of 7-day-old WT and *Rap*^{Osx} littermates. Data represent means ± s.d. **P* < 0.05, *n* = 3. (k) Number of *Ocn*-positive osteoblasts counted along the cortical bone of distal femur from 7-day-old WT and *Rap*^{Osx} littermates. Data represent means ± s.d. **P* < 0.05, *n* = 3. (l) Representative images of alizarin red and calcein double labeling of femur from WT and *Rap*^{Osx} littermates. (m,n) Quantitative parameters mineral apposition rate (MAR) and bone formation rate (BFR) in WT and *Rap*^{Osx} mice. Data represent means ± s.d. **P* < 0.05, *n* = 3

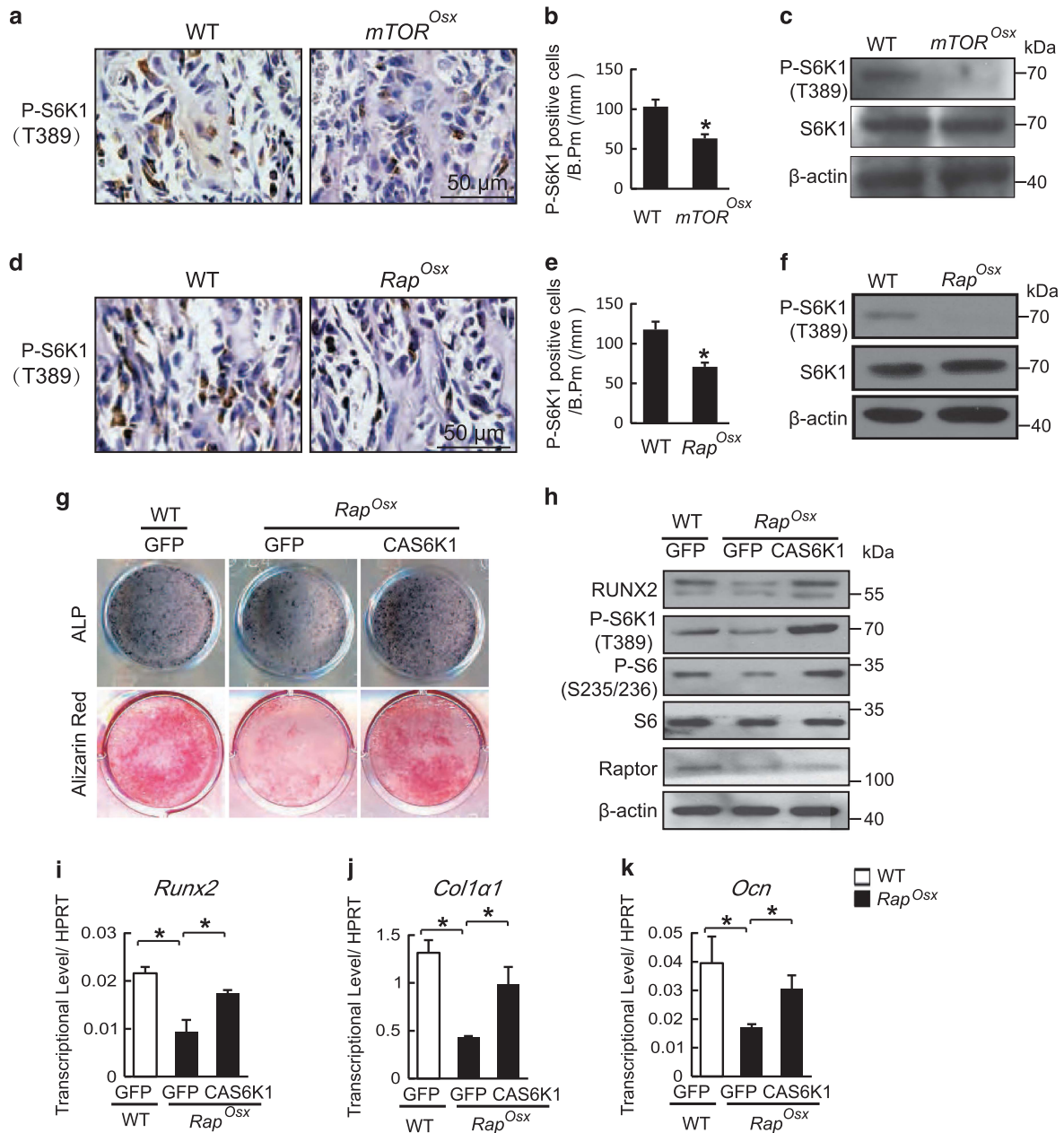


Figure 5 S6K1 is the downstream factor of mTOR/Raptor in osteoblasts. Immunohistochemistry for P-S6K1(T389) in femur from 7-day-old WT and *mTOR^{Osx}* littermates. (a) Number of P-S6K1-positive osteoblast counted in the distal femur of WT and *mTOR^{Osx}* mice. Data represent means \pm s.d. * $P < 0.05$, $n = 3$. (b) Western blot assay for cell lysates from parietal bone of WT and *mTOR^{Osx}* newborn mice. IHC for phospho-S6K1 in femur from P7 WT and *Rap^{Osx}* littermates. (c) Immunohistochemistry for P-S6K1(T389) in femur of 7-day-old WT and *Rap^{Osx}* littermates. (d) Number of P-S6K1-positive osteoblast counted in the distal femur of WT and *Rap^{Osx}* mice. Data represent means \pm s.d. * $P < 0.05$, $n = 3$. (e) Western blot assay for cell lysates from parietal bone of WT and *Rap^{Osx}* newborns. (f) ALP staining and alizarin red staining of WT and *Rap^{Osx}* calvarial cells that were infected with lentivirus expressing CAS6K1 or GFP and induced by osteogenic medium. (g) ALP staining assay for cell lysates from WT and *Rap^{Osx}* calvarial cells that were infected with lentivirus expressing CAS6K1 or GFP followed by osteogenic medium. (i–k) The relative mRNA levels of *Runx2*, *Col1a1* and *Ocn* were quantified by qPCR. Data represent means \pm s.d. * $P < 0.05$, $n = 3$

Materials and Methods

Mice. *mTOR^{fl/fl}* mice bearing loxP sites flanking exons 1–5 of the *mTOR* gene (Stock No: 011009) and *Rap^{fl/fl}* mice bearing loxP sites flanking exons 6 of the *Raptor* gene (Stock No: 013188) were purchased from the Jackson Laboratory (Bar Harbor, Maine, USA). *mTOR^{fl/fl}* mice were crossed with *Osx-cre* mice (*Osx1-GFP::Cre* mice were purchased from the Jackson Laboratory (Stock No: 006361)) to generate *mTOR^{fl/fl};Osx-cre* (*mTOR^{Osx}*) and *mTOR^{fl/+};Osx-cre* (*mTOR^{Osx/+}*) mice. *Rap^{fl/fl}* were crossed with *Osx-cre* mice

to generate *Raptor^{fl/fl};Osx-cre* (*Rap^{Osx}*) and *Raptor^{fl/+};Osx-cre* (*Rap^{Osx/+}*) mice. *Runx2^{+/-}* mice were kindly provided by Professor Gerard Karsenty's laboratory. All mice were C57BL/6 background. All mice were bred and maintained under specific pathogen-free conditions in the institutional animal facility of the Shanghai Institute of Biochemistry and Cell Biology, Chinese Academy of Sciences. All experiments were performed with the protocol approved by the Animal Care and Use Committee of the Shanghai Institute of Biochemistry and Cell Biology.

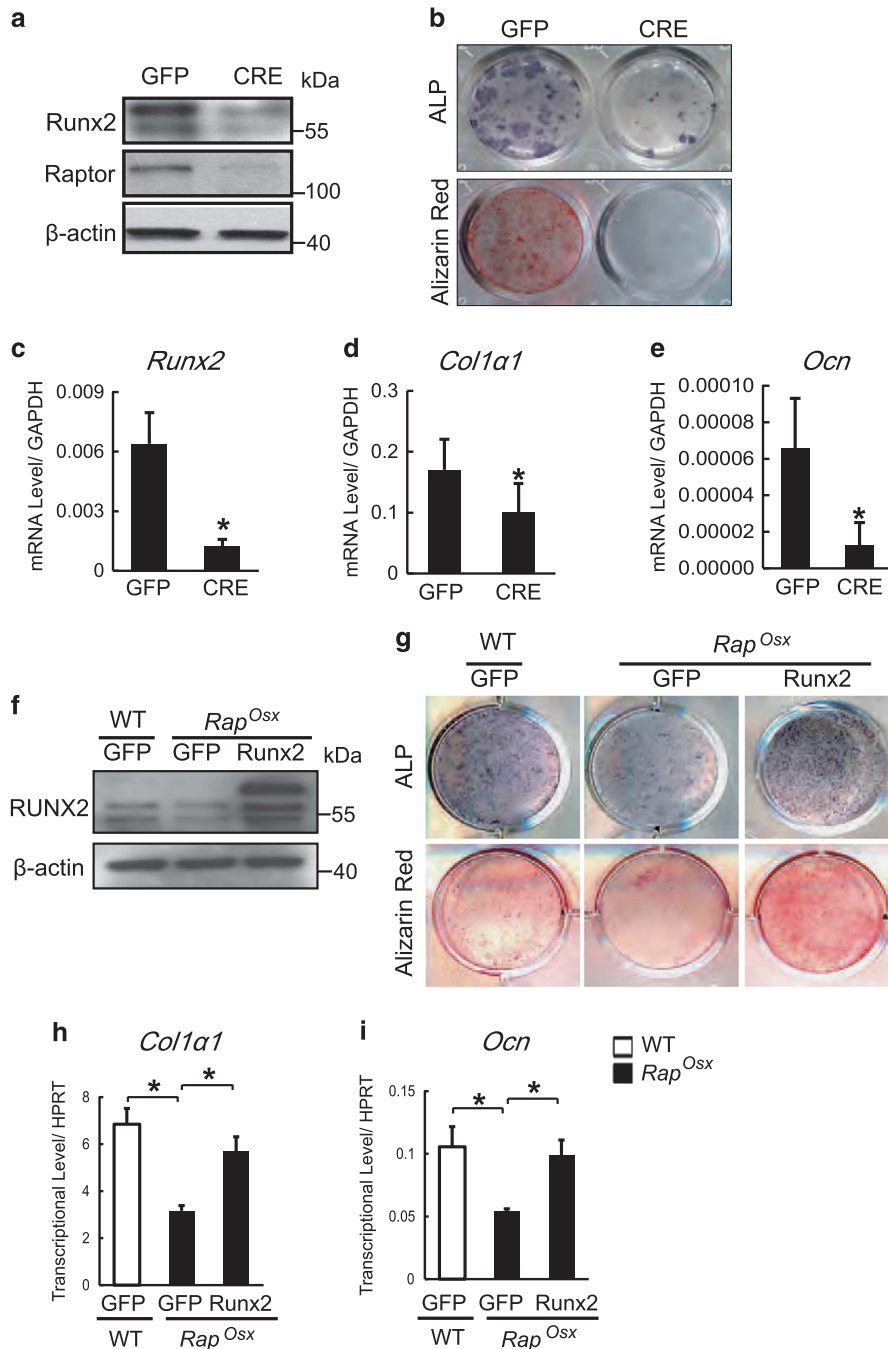


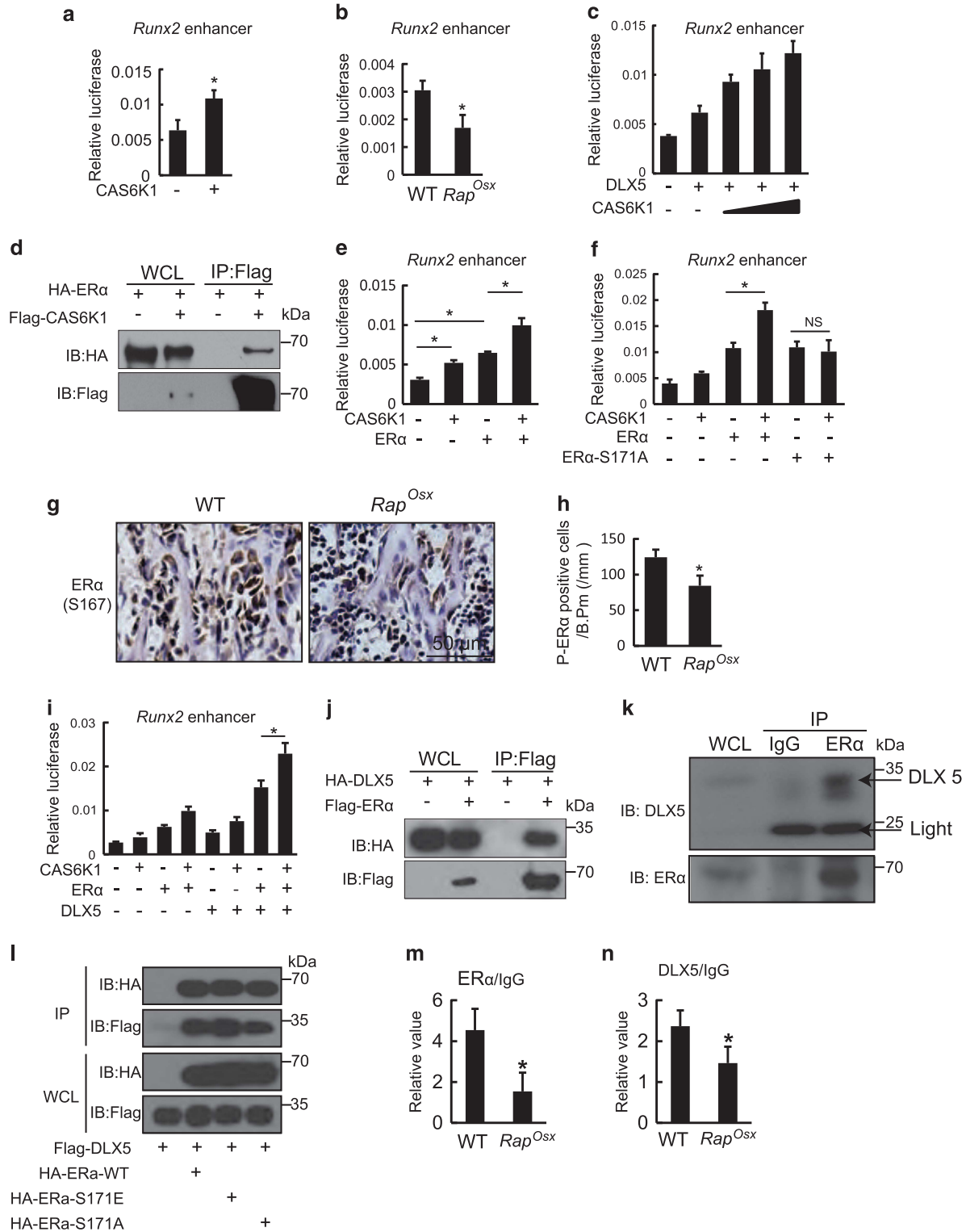
Figure 6 mTOR/Raptor-S6K1 signaling regulates *Runx2* expression in osteoblast. (a) Western blot assay for cell lysates from *Raptor*^{fl/fl} BMSCs that were infected with adenovirus expressing GFP and CRE recombinase. (b) ALP staining and alizarin red staining of BMSCs induced by osteogenic medium. (c–e) The relative mRNA levels of *Runx2*, *Col1a1* and *Ocn* were quantified by qPCR. Data represent means \pm s.d. * $P < 0.05$, $n = 3$. (f) Western blot assay for cell lysates from WT and *Rap*^{Osx} calvarial cells infected with lentivirus expressing Runx2 or GFP. (g) ALP staining and alizarin red staining of WT and *Rap*^{Osx} calvarial cells that were infected with lentivirus expressing Runx2 or GFP and induced by osteogenic medium. (h–i) The relative mRNA levels of *Col1a1* and *Ocn* were quantified by qPCR. Data represent means \pm s.d. * $P < 0.05$, $n = 3$

Skeletal whole mount staining. Skeletal whole mount staining with Alcian blue and Alizarin red was performed as described previously.³² Mice were killed with CO₂, and all skin was carefully removed. Specimens were dehydrated in 95% alcohol for 24 h, followed by cartilage staining in Alcian blue solution for 42 h at 37 °C. After staining, specimens were washed twice in 95% alcohol for 2 h, cleared in 1% KOH for 5 h and stained in Alizarin red solution for 1 h. They were then cleared through 20, 50, and 80% glycerine in 1% KOH, then stored in glycerine.

X-ray and micro-CT analysis. Four-week-old mice were anesthetized with chloral hydrate and subjected to X-ray scanning at 30 KV (Faxitron X-ray, Tucson, AZ, USA). Skulls of 4-week-old and 6-month-old WT and *Rap*^{Osx} mice were used for micro-CT analysis (μ CT80, SCANCO Medical AG, Bassersdorf, Switzerland) with a 10- μ m voxel size. The femur of 4-week-old *mTOR*^{Osx}, *mTOR*^{Osx/+}, *Rap*^{Osx}, *Rap*^{Osx/+x} mice, 6-month-old *Rap*^{Osx} mice and corresponding WT littermates were collected for micro-CT scanning with a 10- μ m voxel size. One hundred slices (total

1 voxel size. One hundred slices (total 1lected for micro-CT scanning witrabecular microarchitecture parameters including bone volume fraction (BV/TV), trabecular thickness (Tb.Th) and trabecular number (Tb.N.) following the introductions of the manufacturer.^{33,34} Fifty slices from the middle of the femur were used to analyze cortical thickness (Ct.Th).³⁵

Histological analysis. Femurs from 7-day-old and 4-week-old mice were fixed in 4% paraformaldehyde for 48 h followed by decalcification in 10% EDTA for 2–4 weeks. Specimens were embedded in paraffin then stained with hematoxylin–eosin and TRAP (Sigma, St. Louis, MO, USA) according to previously described methods.^{36,37}



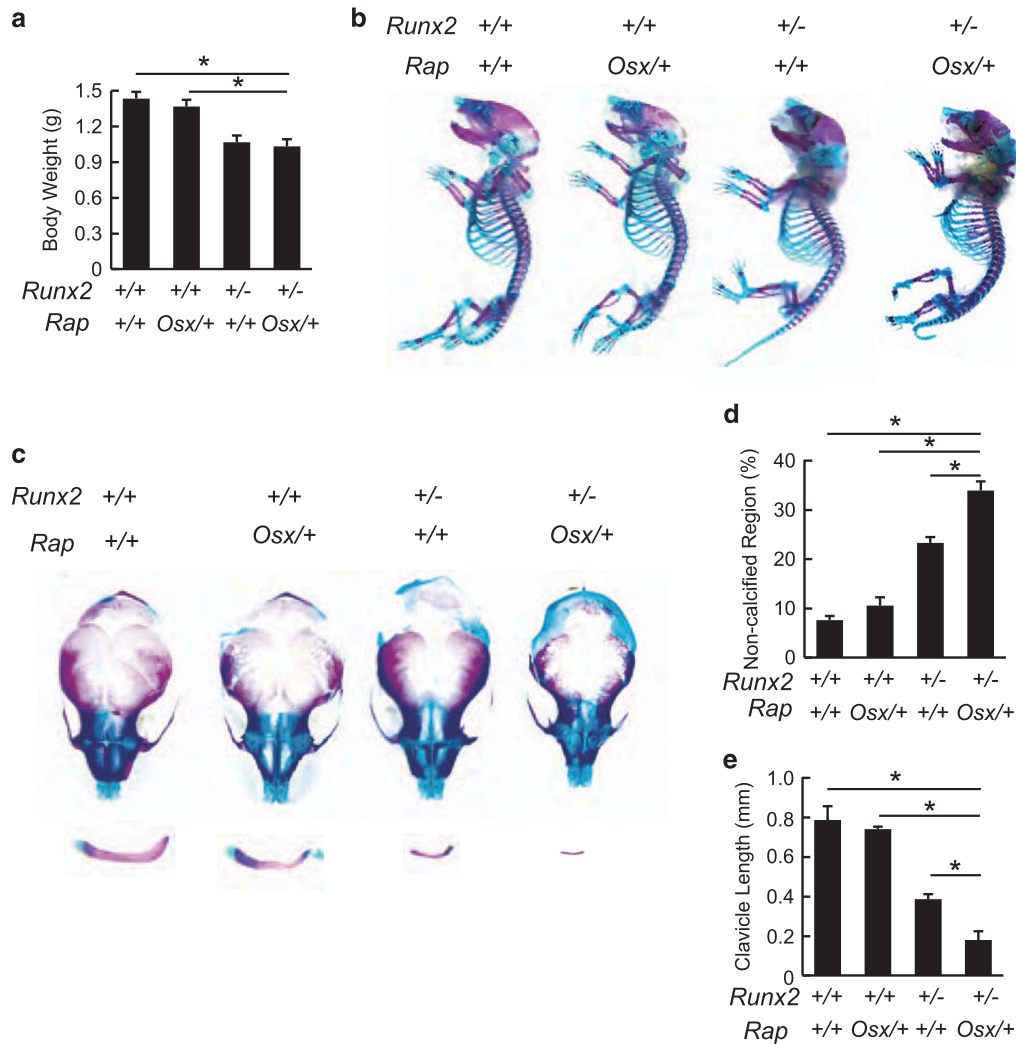


Figure 8 mTORC1 genetically interact with *Runx2*. (a) Body weight analysis of neonatal WT, *Rap*^{Osx/+}, *Runx2*^{+/-}, and *Rap*^{Osx/+}*Runx2*^{+/-} mice. (b) Alcian blue and alizarin red stained skeletal preps of neonatal WT, *Rap*^{Osx/+}, *Runx2*^{+/-}, and *Rap*^{Osx/+}*Runx2*^{+/-} mice. (c) Aggravated clavicular hypoplasia and calvarium hypomineralization in *Rap*^{Osx/+}*Runx2*^{+/-} mice. (d) Relative non-calcified area of calvarial bones of neonatal WT, *Rap*^{Osx/+}, *Runx2*^{+/-}, and *Rap*^{Osx/+}*Runx2*^{+/-} mice. (e) Length of clavicles of neonatal WT, *Rap*^{Osx/+}, *Runx2*^{+/-}, and *Rap*^{Osx/+}*Runx2*^{+/-} mice. Data represent means \pm s.d. **P* < 0.05, *n* = 3

Figure 7 S6K1 regulates *Runx2* expression via its enhancer. (a) Effects of CAS6K1 on *Runx2* enhancer activity. 3X 89 bp *Runx2* enhancer core sequence-driven luciferase reporter and pRL-TK were co-transfected with or without CAS6K1 in C3H10T1/2 cells. Data represent means \pm s.d. **P* < 0.05, *n* = 3. (b) Effects of Raptor deficiency on *Runx2* enhancer activity. 3X 89 bp *Runx2* enhancer core sequence-driven luciferase reporter and pRL-TK were co-transfected in WT and *Rap*^{Osx} calvarial cells. Data represent means \pm s.d. **P* < 0.05, *n* = 3. (c) CAS6K1 promoted DLX5-induced *Runx2* enhancer activity. 3X 89 bp *Runx2* enhancer core sequence-driven luciferase reporter and pRL-TK were co-transfected with DLX5 and different concentration of CAS6K1 in C3H10T1/2 cells. Data represent means \pm s.d. **P* < 0.05, *n* = 3. (d) Co-immunoprecipitation analysis of S6K1 and ER α . Flag-CAS6K1 and HA-ER α expression constructs were co-transfected in 293T cells for 48 h and co-immunoprecipitation analysis was performed. (e) CAS6K1 promoted ER α -induced *Runx2* enhancer activity. 3X 89 bp *Runx2* enhancer core sequence-driven luciferase reporter and pRL-TK were co-transfected with ER α and CAS6K1 in C3H10T1/2 cells. Data represent means \pm s.d. **P* < 0.05, *n* = 3. (f) Effects of mutated ER α of S6K1 phosphorylation motif on *Runx2* enhancer activity. Luciferase assay was performed by co-translating CAS6K1 plasmid with either ER α or ER α S171A, the later one could not be phosphorylated by S6K1. Data represent means \pm s.d. **P* < 0.05, NS, *P* > 0.05 *n* = 3. (g) Immunohistochemistry for P-ER α (S167) in femur from 7-day-old WT and *Rap*^{Osx} littermates. (h) Number of P-ER α -positive osteoblasts counted in the distal femur of WT and *Rap*^{Osx} mice. Data represent means \pm s.d. **P* < 0.05, *n* = 3. (i) Effects of CAS6K1, DLX5 and ER α on *Runx2* enhancer activity. DLX5 and ER α could synergistically increase the activity of *Runx2* enhancer and CAS6K1 could further promote the effects. Data represent means \pm s.d. **P* < 0.05, *n* = 3. (j) Co-immunoprecipitation analysis of ER α and DLX5. Flag-ER α and HA-DLX5 expressing plasmid were co-transfected into 293T cells. After 48 h, immunoprecipitation was performed with whole cell lysate and followed by western blot assay with indicated antibodies. (k) Co-immunoprecipitation analysis of ER α and DLX5 in calvarial osteoblasts. Immunoprecipitation of ER α and IgG was performed with whole cell lysate of calvarial osteoblasts and followed by western blot assay with DLX5 and ER α . (l) Co-immunoprecipitation analysis of DLX5 with ER α and phosphorylation site mutant ER α . Flag-DLX5 was co-transfected with HA-ER α , HA-ER α -S171E or HA-ER α -S171A respectively in 293T cells for 48 h. Immunoprecipitation of Flag and HA was confirmed respectively and western blot assay with indicated antibodies. (m) CHIP-qPCR analysis of ER α in *Runx2* enhancer region using WT and *Rap*^{Osx} calvarial osteoblasts. Data represent means \pm s.d. **P* < 0.05, *n* = 3. (n) CHIP-qPCR analysis of DLX5 in *Runx2* enhancer region using WT and *Rap*^{Osx} calvarial osteoblasts. Data represent means \pm s.d. **P* < 0.05, *n* = 3

Immunohistochemical staining was performed following a previously described protocol.³⁷ Sections were de-waxed and rehydrated. A solution of 3% H₂O₂ was used to block the activity of endogenous peroxidase. Antigen retrieval was performed with protease K at 37 °C for 15 min. Antibodies to Runx2 (1:200, Santa Cruz Biotechnology, Santa Cruz, CA, USA) and P-S6K1 (T389, 1:200, Merck Millipore, Darmstadt, Germany), P-ER α (S167, 1:200, ABclonal, Boston, MA, USA) were added and incubated overnight at 4 °C. Corresponding biotinylated secondary antibodies were then added and incubated for 1 h at room temperature, followed by color development with an ABC kit (Vector Labs, Peterborough, UK). We counted the number of Runx2-, P-S6K1- and P-ER α -positive cells along the trabecular bone of the distal femur excluding the area within 0.25 mm from the growth plate.

In situ hybridization was performed as previously described.³⁷ Briefly, DIG-labeled RNA probes were used to detect mRNA expression in femurs of 7-day-old *mTOR^{Osx}*, *Rap^{Osx}* and corresponding WT littermates. Probes used in this study: probes for mouse *Col1 α 1* (nucleotides 4466-4783, NM_007742, subcloned in pBlueScript), probes for mouse *Ocn* (nucleotides 39-342, NM_007541, subcloned in pBlueScript). After hybridization, probes were visualized by anti-DIG biotin-conjugated antibody and an ABC kit (Vector Labs). Then, samples were counterstained with hematoxylin. We counted *Col1 α 1*-positive cells along trabecular bone of the distal femur excluding the area within 0.25 mm from the growth plate and *Ocn*-positive cells along cortical bone of the distal femur.

Cell culture. Four-week-old *Raptor^{fl/fl}* mice were killed and the hindlimbs were collected. Bone marrow cells were washed out of the long bones and centrifuged at 500 \times g for 10 min. The collected BMSCs were cultured in α -MEM with 10% fetal calf serum and 1% penicillin/streptomycin. After 14 days, BMSCs were reseeded at 2.5 \times 10⁵/cm². Twenty-four hours later, BMSCs were infected with adenovirus expressing either CRE recombinase or GFP at a MOI of 10. Then, BMSCs were cultured in osteogenic medium (α -MEM with 10% FBS and 1% penicillin/streptomycin, 100 nM dexamethasone, 50 μ M L-ascorbic acid, and 10 mM β -glycerophosphate) until required.

Parietal bones of P5 mice (*mTOR^{Osx}*, *Rap^{Osx}* and WT) were digested in 1 mg/ml collagenase (Sigma) and 2 mg/ml Dispase II (Sigma) in α -MEM for 5 min, three times. The released calvarial cells were cultured in α -MEM with 10% FBS and 1% penicillin/streptomycin. After 7 days, calvarial cells were reseeded at 5 \times 10⁴/cm² and cultured in osteogenic medium. For overexpression of CAS6K1 and Runx2, *Rap^{Osx}* calvarial cells were infected with lentivirus expressing CAS6K1 or Runx2. At the same time WT and *Rap^{Osx}* calvarial cells infected with lentivirus expressing GFP were used as control groups. Then these cells were cultured in osteogenic medium.

Alkaline phosphatase staining and alizarin red staining. ALP assay was performed after 7 days of osteoblast differentiation according to the specification of the manufacturer (Beyotime Institute of Biotechnology, Shanghai, China). Mineralized nodule formation was detected by Alizarin red staining 14 days after osteoblast differentiation (Cyagen Biosciences, Santa Clara, CA, USA).

Quantitative PCR (qPCR). Total RNA was extracted from osteoblasts differentiated from BMSCs after 7 days and from calvarial cells using TRIzol, following a standard protocol (Invitrogen, Carlsbad, CA, USA). An aliquot of 500 ng RNA was reverse-transcribed to cDNA using TaKaRa PrimeScript Reverse Transcriptase (TaKaRa Bio Inc., Shiga, Japan). qPCR was performed using a SYBR green mixture (TaKaRa) to detect expression of osteogenic genes. Primers used in this study: *Hprt*-F: 5'-GTTAAGCAGTACAGCCCAAA-3', *Hprt*-R: 5'-AGGG CATATCCAACAACAACACTT-3', β -actin-F: 5'-GTGACGTTGACATCCGTAAGA-3', β -actin-R: 5'-GCCGGACTCATCGTACTCC-3', *Runx2*-F: 5'-CCAACCGAGTCATTT AAGGCT-3', *Runx2*-R: 5'-GCTCAGTCGCTCATCTTG-3', *Col1 α 1*-F: 5'-GCTCC TCTTAGGGGCCACT-3', *Col1 α 1*-R: 5'-CCACGTCTCACCATTGGGG-3', *Ocn*-F: CTTGGTGACACCTAGCAGA-3', *Ocn*-R: 5'-CTCCCTCATGTTGTCCCT-3'.

Plasmids. cDNA of S6K1, ER α and DLX5 were cloned into a phage-based plasmid. Constitutively active S6K1 was constructed following previously described methods by converting Thr³⁹⁰ to glutamic acid.³⁸ Non-phosphorylatable ER α was constructed by converting Ser¹⁷¹ into alanine and constitutively phosphorylated ER α was constructed by converting Ser¹⁷¹ into glutamic acid. A 3X 89 bp Runx2 enhancer core sequence was synthesized (by Genescript, Piscataway, NJ, USA) and cloned into a phage-based luciferase reporter.²³ The Runx2 plasmid was a gift from Dr. Gerard Karsenty's lab. The Runx2 promoter-driven pGL3-based luciferase reporter was kindly provided by Dr. Zhang Feng.³⁹

Transient transfection and luciferase reporter assay. Mouse MSC C3H10T1/2 cells were seeded at 4 \times 10⁴ cells/well into a 12-well plate, allowed to settle overnight, then transfected using PEI with a luciferase reporter plasmid and Renilla luciferase (Promega, Madison, WI, USA) along with various combinations of expression plasmids as indicated. Empty expression vector plasmids were used as required to make up the total amount of transfected DNA. At 48 h post-transfection, the cells were lysed with lysis buffer (1% NP-40, 10% glycerol, 135 mM NaCl, 20 mM Tris, pH 8.0) with protease inhibitor and lysates were used for the dual-luciferase reporter assay (Promega). In our study, promoter activity was expressed as relative light units normalized to the activity of cotransfected Renilla luciferase.

Co-immunoprecipitation and western blot. For western blot analysis of parietal bone, total proteins were obtained from P0 mice with SDS buffer (TaKara). For western blot analysis of BMSCs and calvarial cells, total proteins were obtained from BMSCs and calvarial cells after 7 days of differentiation in osteogenic medium. Proteins (60 μ g of parietal bone protein or 30 μ g of cells) were separated by 10% SDS-PAGE followed by western blotting according to a standard protocol. Antibodies used were: mTOR (Cell Signaling Technology, Danvers, MA, USA), Raptor (Cell Signaling Technology), P-S6K1 (T389, Merck Millipore), S6K1 (Cell Signaling Technology), P-S6 (S235/236, Cell Signaling Technology), S6 (Cell Signaling Technology), Runx2 (Santa Cruz Biotechnology), β -actin (Santa Cruz Biotechnology).

CoIP was performed following a method previously described.³⁷ Briefly, 293T cells were seeded into a 10 cm dish at a concentration of 3 \times 10⁶ cells/dish and allowed to settle overnight. At 48 h post-transfection with PEI, cells were lysed and whole cell lysates were used for immunoprecipitation by Flag or HA antibody (Sigma) at 4 °C overnight. Western blot assay was performed with the indicated antibodies (anti-HA and anti-Flag, Sigma). For CoIP analysis of ER α and DLX5 in calvarial osteoblast, whole cell lysates were incubated with IgG and ER α (Sangon Biotech, Shanghai, China) at 4 °C overnight. Western blot assay was performed with DLX5 (Abcam, Cambridge, UK) and anti-ER α (Abcam).

Chromatin immunoprecipitation (ChIP) and qPCR. CHIP analysis in WT and *Rap^{Osx}* calvarial osteoblast was performed following by an Enzymatic Chromatin Immunoprecipitation kit (Cell Signaling Technology) following the instructions of the manufacturer. Briefly, calvarial osteoblasts were cross-linked with 1% formaldehyde for 10 min at room temperature followed by quenched with glycine. Chromatin digestion was performed to obtain DNA fragments from 150 bp to 900 bp by Micrococcal Nuclease. Immunoprecipitation was performed with DLX5 (Abcam) and ER α (Abcam), and IgG was used as a negative control. Precipitated DNA was detected by qPCR with specific primers. Primers for Runx2 enhancer: F: 5'-CTGCTTTAGGTAGAGGGCTT-3', R: 5'-AATCAGAGTGGAGTCTCAGC-3'.

Statistical analysis. All quantitative data are presented as mean \pm s.d. from at least three independent samples. Student's *t*-test was used for statistical evaluations of two group comparisons. Statistical analysis with more than two groups was performed with one-way analysis of variance (ANOVA). *P* < 0.05 was considered statistically significant.

Conflict of Interest

The authors declare no conflict of interest.

Acknowledgements. The authors thank Drs Gerard Karsenty, Feng Zhang, Minghan Tong for kindly providing reagents. We thank the members of the Zou lab for useful discussions. This work was supported in part by grants from 973 Program from the Chinese Ministry of Science and Technology (MOST) (2014CB964704 and 2015CB964503), the Science and Technology Commission of Shanghai (124119b0101), the National Natural Science Foundation of China (NSFC) (31371463, 31501170, 81371121 and 81570950), the Strategic Priority Research Program of the Chinese Academy of Sciences, Grant No. XDB19000000, Shanghai Summit & Plateau Disciplines, the 'Chen Xing' project from Shanghai Jiaotong University and WZ is a scholar of the 'National 1000 Young Talents Program of China' and 'the National Science Fund for Excellent Young Scholars' (NSFC) (81322027).

Author contributions

Conceived and designed the experiments: JW, WZ. Performed the experiments: QD, ZX, NN, XM, SZ, FX. Analyzed the data: QD, WZ. Contributed reagents/materials/analysis tools: XZ, LJ. Wrote the paper: QD, WZ.

1. Harada S, Rodan GA. Control of osteoblast function and regulation of bone mass. *Nature* 2003; **423**: 349–355.
2. Guntur AR, Rosen CJ. The skeleton: a multi-functional complex organ. New insights into osteoblasts and their role in bone formation: the central role of PI3Kinase. *J Endocrinol* 2011; **211**: 123–130.
3. Ducy P, Zhang R, Geoffroy V, Ridall AL, Karsenty G. *Osf2/Cbfa1*: a transcriptional activator of osteoblast differentiation. *Cell* 1997; **89**: 747–754.
4. Otto F, Thornell AP, Crompton T, Denzel A, Gilmour KC, Rosewell IR *et al*. *Cbfa1*, a candidate gene for cleidocranial dysplasia syndrome, is essential for osteoblast differentiation and bone development. *Cell* 1997; **89**: 765–771.
5. Komori T, Yagi H, Nomura S, Yamaguchi A, Sasaki K, Deguchi K *et al*. Targeted disruption of *Cbfa1* results in a complete lack of bone formation owing to maturational arrest of osteoblasts. *Cell* 1997; **89**: 755–764.
6. Mundlos S, Otto F, Mundlos C, Mulliken JB, Aylsworth AS, Albright S *et al*. Mutations involving the transcription factor *CBFA1* cause cleidocranial dysplasia. *Cell* 1997; **89**: 773–779.
7. Bhaskar PT, Hay N. The two TORCs and Akt. *Dev cell* 2007; **12**: 487–502.
8. Nojima H, Tokunaga C, Eguchi S, Oshiro N, Hidayat S, Yoshino K *et al*. The mammalian target of rapamycin (mTOR) partner, raptor, binds the mTOR substrates p70 S6 kinase and 4E-BP1 through their TOR signaling (TOS) motif. *J Biol Chem* 2003; **278**: 15461–15464.
9. Yamnik RL, Digilova A, Davis DC, Brodt ZN, Murphy CJ, Holz MK. S6 kinase 1 regulates estrogen receptor alpha in control of breast cancer cell proliferation. *J Biol Chem* 2009; **284**: 6361–6369.
10. Carnevalli LS, Masuda K, Frigerio F, Le Bacquer O, Um SH, Gandin V *et al*. S6K1 plays a critical role in early adipocyte differentiation. *Dev cell* 2010; **18**: 763–774.
11. Zoncu R, Efeyan A, Sabatini DM. mTOR: from growth signal integration to cancer, diabetes and ageing. *Nat Rev Mol Cell Biol* 2011; **12**: 21–35.
12. Xiang X, Zhao J, Xu G, Li Y, Zhang W. mTOR and the differentiation of mesenchymal stem cells. *Acta Biochim Biophys Sin (Shanghai)* 2011; **43**: 501–510.
13. Singha UK, Jiang Y, Yu S, Luo M, Lu Y, Zhang J *et al*. Rapamycin inhibits osteoblast proliferation and differentiation in MC3T3-E1 cells and primary mouse bone marrow stromal cells. *J Cell Biochem* 2008; **103**: 434–446.
14. Yeh LC, Ma X, Ford JJ, Adamo ML, Lee JC. Rapamycin inhibits BMP-7-induced osteogenic and lipogenic marker expressions in fetal rat calvarial cells. *J Cell Biochem* 2013; **114**: 1760–1771.
15. Lee KW, Yook JY, Son MY, Kim MJ, Koo DB, Han YM *et al*. Rapamycin promotes the osteoblastic differentiation of human embryonic stem cells by blocking the mTOR pathway and stimulating the BMP/Smad pathway. *Stem cells dev* 2010; **19**: 557–568.
16. Fang F, Sun S, Wang L, Guan JL, Giovannini M, Zhu Y *et al*. Neural crest-specific TSC1 deletion in mice leads to sclerotic craniofacial bone lesion. *J Bone Miner Res* 2015; **30**: 1195–1205.
17. Riddle RC, Frey JL, Tomlinson RE, Ferron M, Li Y, DiGirolamo DJ *et al*. Tsc2 is a molecular checkpoint controlling osteoblast development and glucose homeostasis. *Mol Cell Biol* 2014; **34**: 1850–1862.
18. Huang B, Wang Y, Wang W, Chen J, Lai P, Liu Z *et al*. mTORC1 prevents preosteoblast differentiation through the notch signaling pathway. *PLoS Genet* 2015; **11**: e1005426.
19. Chen C, Akiyama K, Wang D, Xu X, Li B, Moshaverinia A *et al*. mTOR inhibition rescues osteopenia in mice with systemic sclerosis. *J Exp Med* 2014; **212**: 73–91.
20. Chen J, Long F. mTORC1 signaling controls mammalian skeletal growth through stimulation of protein synthesis. *Development* 2014; **141**: 2848–2854.
21. Chen J, Long F. mTORC1 signaling promotes osteoblast differentiation from preosteoblasts. *PLoS one* 2015; **10**: e0130627.
22. Martin SK, Fitter S, Dutta AK, Matthews MP, Walkley CR, Hall MN *et al*. Brief report: the differential roles of mTORC1 and mTORC2 in mesenchymal stem cell differentiation. *Stem Cells* 2015; **33**: 1359–1365.
23. Kawane T, Komori H, Liu W, Morishi T, Miyazaki T, Mori M *et al*. *Dlx5* and *mef2* regulate a novel *runx2* enhancer for osteoblast-specific expression. *J Bone Miner Res* 2014; **29**: 1960–1969.
24. Yamnik RL, Holz MK. mTOR/S6K1 and MAPK/RSK signaling pathways coordinately regulate estrogen receptor alpha serine 167 phosphorylation. *FEBS Lett* 2010; **584**: 124–128.
25. Kammerer M, Gutzwiller S, Stauffer D, Delhon I, Seltenmeyer Y, Fournier B. Estrogen Receptor α (ER α) and Estrogen Related Receptor α (ERR α) are both transcriptional regulators of the *Runx2-1* isoform. *Mol Cell Endocrinol* 2013; **369**: 150–160.
26. Melville KM, Kelly NH, Khan SA, Schimenti JC, Ross FP, Main RP *et al*. Female mice lacking estrogen receptor-alpha in osteoblasts have compromised bone mass and strength. *J Bone Miner Res* 2014; **29**: 370–379.
27. Almeida M, Iyer S, Martin-Millan M, Bartell SM, Han L, Ambrogini E *et al*. Estrogen receptor-alpha signaling in osteoblast progenitors stimulates cortical bone accrual. *J Clin Invest* 2013; **123**: 394–404.
28. Guo J-P, Shu S-K, Esposito NN, Coppola D, Koomen JM, Cheng J-Q. IKK ϵ phosphorylation of estrogen receptor α Ser-167 and contribution to tamoxifen resistance in breast cancer. *J Biol Chem* 2010; **285**: 3676–3684.
29. Yan B, Zhang Z, Jin D, Cai C, Jia C, Liu W *et al*. mTORC1 regulates PTHrP to coordinate chondrocyte growth, proliferation and differentiation. *Nat Commun* 2016; **7**: 11151.
30. Polak P, Cybulski N, Feige JN, Auwerx J, Ruegg MA, Hall MN. Adipose-specific knockout of raptor results in lean mice with enhanced mitochondrial respiration. *Cell Metab* 2008; **8**: 399–410.
31. Lou Y, Javed A, Hussain S, Colby J, Frederick D, Pratap J *et al*. A *Runx2* threshold for the cleidocranial dysplasia phenotype. *Hum Mol Genet* 2009; **18**: 556–568.
32. Kelly WL, Bryden MM. A modified differential stain for cartilage and bone in whole mount preparations of mammalian fetuses and small vertebrates. *Stain Technol* 1983; **58**: 131–134.
33. Yuan Q, Jiang Y, Zhao X, Sato T, Densmore M, Schuler C *et al*. Increased osteopontin contributes to inhibition of bone mineralization in FGF23-deficient mice. *J Bone Miner Res* 2014; **29**: 693–704.
34. Liu W, Zhou L, Zhou C, Zhang S, Jing J, Xie L *et al*. GDF11 decreases bone mass by stimulating osteoclastogenesis and inhibiting osteoblast differentiation. *Nat Commun* 2016; **7**: 12794.
35. Guo Y, Sun N, Duan X, Xu X, Zheng L, Seriwatanachai D *et al*. Estrogen deficiency leads to further bone loss in the mandible of CKD mice. *PLoS one* 2016; **11**: e0148804.
36. Andersson GN, Marks S. Tartrate-resistant acid ATPase as a cytochemical marker for osteoclasts. *J Histochem Cytochem* 1989; **37**: 115.
37. Zou W, Greenblatt MB, Brady N, Lotinun S, Zhai B, de Rivera H *et al*. The microtubule-associated protein DCAMK1 regulates osteoblast function via repression of *Runx2*. *J Exp Med* 2013; **210**: 1793–1806.
38. Xia T, Cheng Y, Zhang Q, Xiao F, Liu B, Chen S *et al*. S6K1 in the central nervous system regulates energy expenditure via MC4R/CRH pathways in response to deprivation of an essential amino acid. *Diabetes* 2012; **61**: 2461–2471.
39. Zhang F, Xu L, Xu Q, Li D, Yang Y, Karsenty G *et al*. JMJD3 promotes chondrocyte proliferation and hypertrophy during endochondral bone formation in mice. *J Mol Cell Biol* 2015; **7**: 23–34.



This work is licensed under a Creative Commons Attribution-NonCommercial-NoDerivs 4.0 International License. The images or other third party material in this article are included in the article's Creative Commons license, unless indicated otherwise in the credit line; if the material is not included under the Creative Commons license, users will need to obtain permission from the license holder to reproduce the material. To view a copy of this license, visit <http://creativecommons.org/licenses/by-nc-nd/4.0/>

© The Author(s) 2017

Supplementary Information accompanies this paper on *Cell Death and Differentiation* website (<http://www.nature.com/cdd>)